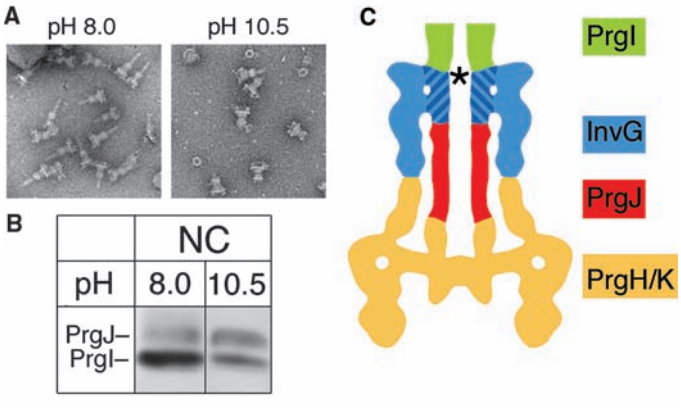


**Fig. 4.** PrgJ is recruited as a structural component to the base during needle assembly. (**A**) Electron micrographs of needle complexes before (pH 8.0) and after subjection to pH 10.5 to affect needle disassembly. (**B**) Western blot analysis of untreated and pH 10.5–treated needle showed that elevated pH drastically diminished the amount of the needle protein PrgI, as expected based on the images shown in (A), but did not affect the amount of PrgJ, which, therefore, must be located within the base. (**C**) Model cartoon summarizing the proposed organization of the five major structural components of the needle complex: PrgH, PrgK, PrgJ, InvG, and PrgI. Hatched coloring indicates the uncertainty in the exact boundaries of PrgI, InvG, and PrgJ. The asterisk marks the location where the secretion tunnel markedly narrows at the entry point to the needle, which attaches to the outermost periphery of the base through a contact with InvG.

base (movie S2). These changes were complemented by an outward movement of OR2 and a drastic remodeling that flattened the septum, sealing the apical side of the base, against OR2 during needle assembly (Fig. 3, A and B; movie S2). This rearrangement of the septum is essential for creation of the secretion channel and transformed part of InvG from being a barrier into forming two scaffolds that enable assembly of the needle and the inner rod. Like the socket structure at the basal end of the chamber, these new scaffolds likely serve as adaptors, accommodating the symmetry mismatches between the base, the needle, and the inner rod.

The diameter of the secretion channel narrowed at the outermost boundary of the base before opening to the central channel of the needle substructure (Figs. 3A and 4C). This change of diameter could not be reconciled with the helical symmetry of the filamentous needle, formed by PrgI, and suggested that the rod inside the base was formed by another protein. The most likely candidate to form the inner rod was PrgJ, which has been detected in needle-complex preparations (*10*, *13*). To test this hypothesis, we subjected purified needle complexes to an elevated pH. This treatment caused disassembly of the needle filament (Fig. 4A), yet did not affect the amount of PrgJ (Fig. 4B), which therefore must be localized within the base. Moreover, quantitative amino acid analysis revealed that in needle complexes, PrgJ and PrgI were present in 1:6 molar ratios (fig. S3), which was too high to support previous models suggesting that PrgJ exclusively caps the tip of the needle (*13*, *15*) [such a ratio should be at least 1:24 (*6*)].

Our structural analysis of the needle complex of the *S. typhimurium* TTSS revealed that the needle attaches to the base at its outermost periphery and identified a new substructure formed by InvG and PrgJ. Moreover, visualization of conformational changes that contribute to reprogramming of TTSS to secrete effector proteins provides essential insights into structure-function relationships of this important virulence factor.

### References and Notes

1. G. R. Cornelis, F. Van Gijsegem, *Annu. Rev. Microbiol.* **54**, 735 (2000).
2. J. E. Galán, A. Collmer, *Science* **284**, 1322 (1999).
3. T. Kubori *et al.*, *Science* **280**, 602 (1998).
4. T. Kubori, A. Sukhan, S. I. Aizawa, J. E. Galán, *Proc. Natl. Acad. Sci. U.S.A.* **97**, 10225 (2000).
5. J. E. Galán, R. Curtiss III, *Proc. Natl. Acad. Sci. U.S.A.* **86**, 6383 (1989).
6. Materials and methods are available as supporting material on *Science* Online.
7. T. C. Marlovits, T. Kubori, J. E. Galán, V. Unger, unpublished results.
8. M. Valle *et al.*, *EMBO J.* **21**, 3557 (2002).
9. S. Yang *et al.*, *J. Mol. Biol.* **321**, 839 (2002).
10. A. Sukhan, T. Kubori, J. E. Galán, *J. Bacteriol.* **185**, 3480 (2003).
11. C. Collazo, J. E. Galán, *Infect. Immun.* **64**, 3524 (1996).
12. A. Sukhan, T. Kubori, J. Wilson, J. E. Galán, *J. Bacteriol.* **183**, 1159 (2001).
13. T. G. Kimbrough, S. I. Miller, *Proc. Natl. Acad. Sci. U.S.A.* **97**, 11008 (2000).
14. J. E. Galán, *Annu. Rev. Cell Dev. Biol.* **17**, 53 (2001).
15. A. Blocker *et al.*, *Mol. Microbiol.* **39**, 652 (2001).
16. We thank D. J. DeRosier and F. Sigworth for helpful discussions about the image processing. We are grateful to the Yale School of Medicine for the support of the Cryo Electron Microscopy Core Facility; N. Grigorieff (Brandeis University) for the use of a computer cluster; and the Howard Hughes Medical Institute Keck Facility at Yale for the quantitative amino acid analysis. Molecular graphics images (Fig. 2) were produced using the UCSF Chimera package from the Computer Graphics Laboratory, University of California, San Francisco (NIH P42 RR-01081). This work was supported by Public Health Service grants GM35433 from the NIH to D. J. DeRosier (supporting D.R.T), AI30492 to J.E.G, and GM66145 to V.M.U. and by a Hellman Family Fellowship to V.M.U. The structure of the Needle Complex has been deposited in the EmDep Database with accession code EMD-1100.

**Supporting Online Material**
www.sciencemag.org/cgi/content/full/306/5698/1040/DC1
Materials and Methods
Figs. S1 to S3
References
Movies S1 and S2

12 July 2004; accepted 3 September 2004

# Tracking SNARE Complex Formation in Live Endocrine Cells

**Seong J. An and Wolfhard Almers***

**Syntaxin, synaptosome-associated protein of 25 kD (SNAP25), and vesicle-associated membrane protein/synaptobrevin are collectively called SNAP receptor (SNARE) proteins, and they catalyze neuronal exocytosis by forming a "core complex." The steps in core complex formation are unknown. Here, we monitored SNARE complex formation in vivo with the use of a fluorescent version of SNAP25. In PC12 cells, we found evidence for a syntaxin-SNAP25 complex that formed with high affinity, required only the amino-terminal SNARE motif of SNAP25, tolerated a mutation that blocks formation of other syntaxin-SNAP25 complexes, and assembled reversibly when $Ca^{2+}$ entered cells during depolarization. The complex may represent a precursor to the core complex formed during a $Ca^{2+}$-dependent priming step of exocytosis.**

The fusion of secretory vesicles with the plasma membrane is essential for the release of transmitters from neurons and of hormones from endocrine cells. It is catalyzed by the combination of syntaxin (Syx) and SNAP25 on the plasma membrane with vesicle-associated membrane protein/synaptobrevin (Syb) on vesicles. The three proteins, collectively called SNAREs, assemble into an exocytic core complex that pulls membranes close together (*1*) by forming a twisted bundle of four parallel α helices (*2*). In this coiled coil, one helix is formed by Syx, another by Syb, and one each by the two SNARE motifs of SNAP25. The core complex almost certainly forms in steps. Indeed, partial SNARE complexes can form in solution (*3*), but it is unclear which of them, if any, are core

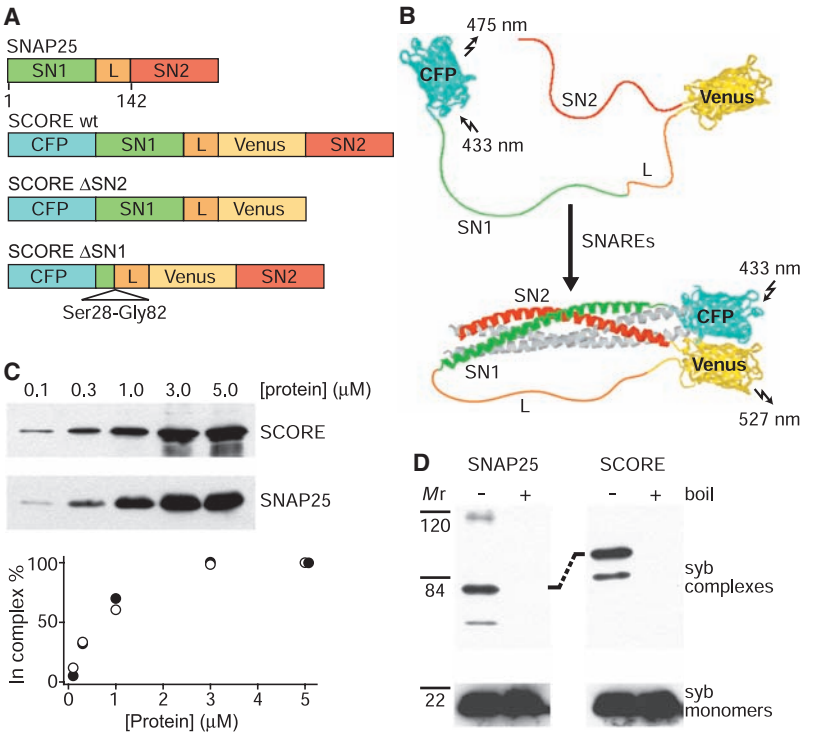


**Fig. 1.** SCORE. (**A**) Domain structure of SNAP25, SCORE, and its variants. ΔSN2 lacked the last 65 C-terminal residues, whereas ΔSN1 lacked Ser[28] through Gly[82]. Venus inserted between residues 141 and 142. (**B**) Schematic diagrams of SCORE, uncomplexed or in the four-helix bundle of the core complex (*2*). The N-terminal region of Syx was omitted for clarity. (**C**) SNARE complex formation by SNAP25 and SCORE. Full-length Syx was fused to glutathione-*S*-transferase (GST). Glutathione sepharose beads coated with GST-Syx (0.5 μM) were mixed with Syb (1 μM) and the indicated amounts of either SNAP25 or SCORE. After overnight incubation at 4°C, beads were washed and analyzed by SDS-polyacrylamide gel electrophoresis (SDS-PAGE) and immunoblotting with a SNAP25 antibody (top). Density of bands normalized to values obtained at 5 μM SCORE or SNAP25 (bottom). (**D**) SDS resistance of native and SCORE-containing SNARE complexes. Full-length Syx and Syb were incubated overnight with SNAP25 or SCORE (all 1 μM), placed in sample buffer containing SDS (4% w/v) at room temperature or boiled, and then analyzed by SDS-PAGE and immunoblotting with a Syb antibody. The dashed line highlights the difference in mobility of SNAP25- and SCORE-containing core complexes. *M*r, relative molecular mass (κ). In (C) and (D), SCORE contained yellow fluorescent protein in place of Venus; the two fluorophores differ by five amino acids.

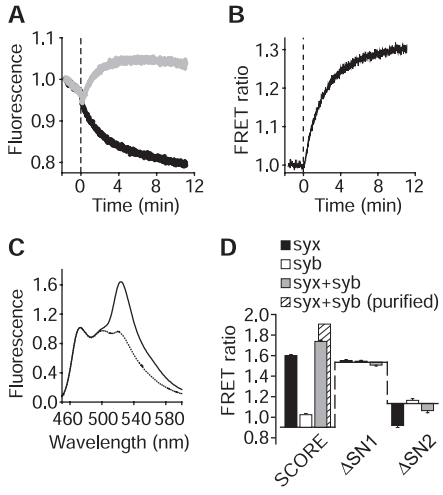


**Fig. 2.** Spectral properties of SCORE-based probes. (**A**) Fluorescence of SCORE after the addition of soluble Syx-H3 (vertical dashed line). Cyan (black) and yellow fluorescence (gray) were measured simultaneously by fluorimetry (excitation 433 nm). Recombinant Syx-H3 was added to a stirred 1-ml sample of recombinant SCORE (2 μM) to a final concentration [Syx-H3] = 4 μM (mixing time 3 to 4 s). Three runs normalized to their initial values and averaged. (**B**) FRET ratio (yellow/cyan) of traces in (A), normalized to their initial values. The trace rises with a time constant of 120 s. (**C**) Emission spectra of recombinant SCORE after overnight incubation at 4°C either by itself (2 μM, dotted line) or with 8 μM Syx-H3 (solid line). Spectra from three reactions were normalized to their values at 475 nm (near CFP emission peak) and averaged. (**D**) FRET ratio (emission ratio 527/475 nm) from experiments similar to (C). SCORE and its mutants (2 μM) were incubated overnight with Syx-H3 (8 μM) or soluble Syb(1–92) (8 μM), or with 8 μM Syx-H3 plus 8 μM Syb(1–92). Horizontal lines indicate intrinsic FRET ratio without added SNAREs, and the height of the bars indicates SNARE-induced changes. Cross-hatched bar, purified core complex. Error bars show mean ± standard error.

complex precursors in vivo (*4*–*6*). The steps in core complex formation are important because their regulation may contribute to short-term synaptic plasticity.

To better understand SNARE complex formation in living cells, we made a fluorescent SNAP25 that reports entry into SNARE complexes by intramolecular fluorescence resonance energy transfer (FRET) (*7*). In SNAP25, a linker that is ~60 amino acids long connects two SNARE motif regions, SN1 and SN2 (Fig. 1A). SN1 and SN2 are unstructured when SNAP25 is solitary (*8*). However, when SNAP25 forms a core complex with the SNARE motifs of Syb and Syx (*2*) or a binary complex with two copies of Syx (*8*–*10*), then SN1 and SN2 fold as parallel helices within a four-helix bundle, and their N termini approach closely. To detect their approach, cyan fluorescent protein (CFP) was inserted as a FRET donor, and the fluorescent protein Venus (*11*) was inserted as a FRET acceptor (Fig. 1B). The resulting construct, termed SNARE complex reporter (SCORE) (Fig. 1A), was as effective as SNAP25 in forming complexes with full-length versions of Syx and Syb (Fig. 1C). Such complexes were resistant to SDS (Fig. 1D), as is the native SNARE core complex.

When recombinant SCORE was mixed with the soluble SNARE motif of Syx (Syx-H3), the fluorescence of CFP diminished, whereas that of Venus increased (Fig. 2A), characteristic of FRET. The ratio of yellow and cyan fluorescence increased with half-time $t_{1/2}$ = 105 s (Fig. 2B) as the two fluorophores approached, presumably signaling formation of the binary complex $(Syx\text{-}H3)_2$-SCORE [$t_{1/2}$ = 60 s by circular dichroism (*12*)]. Overnight incubation with Syx-H3 caused a large increase of fluorescence at 527 nm, corresponding to a 78% increase in FRET ratio (Fig. 2C). The FRET increase was much smaller with a soluble Syb mutant containing only the first 92 amino acids [Syb(1–92)], but larger when Syb(1–92) and Syx-H3 were added together, especially when the core complex thus formed was purified (Fig. 2D).

Two deletion mutants of SCORE were examined (Fig. 2D). ΔSN1 lacked SN1 (Fig. 1A) and showed considerable FRET on its own, but no change in FRET when Syx-H3 and Syb(1–92) were added. ΔSN2 lacked SN2, and FRET decreased when Syx-H3 was added (*13*). We conclude that SCORE integrates into SNARE complexes in a manner similar or identical to SNAP25, and that SCORE but not its deletion mutants showed markedly increased FRET under

Vollum Institute L-474, Oregon Health Sciences University, 3181 Southwest Sam Jackson Park Road, Portland, OR 97201, USA.

*To whom correspondence should be addressed. E-mail: almersw@ohsu.edu

conditions in which native SNAREs form four-helix bundles.

To study interactions of Syx with our SCORE-based probes in vivo, we cotransfected PC12 cells with SCORE and with full-length Syx carrying red fluorescent protein [mRFP (*14*)] at its extracellular end. Each cell was viewed as a compartment in which probes and Syx could interact (*15*) and cause FRET, and in which their concentrations could be measured fluorimetrically. Fluorescence was excited first for CFP and then for mRFP (Fig. 3A). Because cells expressed probes and Syx-mRFP in amounts and proportions varying over a nearly 100-fold range, we first selected cells with low probe concentration. With SCORE, the FRET ratio increased with the concentration of Syx-mRFP (Fig. 3B), approaching the value obtained for purified core complex in vitro (termed "full FRET" below). Full FRET suggests the formation of a $(Syx)_2$-SCORE four-helix bundle. In cells expressing ΔSN1 (Fig. 3C, red triangles), FRET was higher than with SCORE but entirely independent of the concentration of Syx, as in Fig. 2D.

With ΔSN2, however, Syx increased FRET (Fig. 3C, black circles), in contrast to our result in vitro. As the concentration of Syx rose, FRET rose to a peak and then declined. Thus, at low concentrations, Syx entered into a complex with ΔSN2 causing partial FRET, but higher Syx concentration promoted another, "silent" complex that produced little or no FRET. Because partial FRET is due to a Syx-SN1 complex, we wondered whether the mutation $Gly^{43}\rightarrow Asp^{43}$ (G43D) in the SN1 domain prevents partial FRET. This mutation (*16*) prevents the assembly of the only other known complex between Syx and SN1, a four-helix bundle of stoichiometry $(Syx\text{-}SN1)_2$ (*17*). However, ΔSN2-G43D not only failed to abolish partial FRET, but retained it even at the highest Syx concentration tested (Fig. 3D), as if formation of the silent complex were now blocked. Partial FRET was seen to develop at low Syx concentration and then saturate. Saturation occurred at a lower concentration than for full FRET (Fig. 3B). Thus, the complex causing partial FRET formed with higher affinity.

A Syx mutant lacking its N-terminal domain, Syx-ΔNT-mRFP, gave the same results as the wild type with all probes. The N-terminal domain can keep Syx in a closed conformation that is unable to bind SNAREs (*18*), but evidently did not interfere with complex formation after 24 hours of coexpression, consistent with (*19*). An analysis also including cells expressing higher concentrations of SCORE probes and Syx-mRFP constructs (Fig. 3, E to G), confirmed the major results of Fig. 3, B to D.

In cells transfected with SCORE probes alone, the amount of Syx can become rate limiting, and the FRET ratio is expected to be highest in cells expressing low amounts of the SCORE. Indeed, as the concentration of SCORE was raised, the FRET ratio first increased and then diminished as an endogenous pool of Syx became saturated (Fig. 3H). Similar results were obtained with ΔSN2 and ΔSN2-G43D but not with ΔSN1 (*20*). Apparently, the FRET signal with endogenous Syx arose predominantly from partial FRET.

In summary, SCORE generated strong intramolecular FRET, both when it entered exocytic core complexes and under conditions favoring $Syx_2$-SCORE complexes. In vitro, FRET failed to increase when either of the two SNARE motifs was missing. In vivo, however, ΔSN2 generated Syx-mediated partial FRET. Partial FRET and its resistance to the G43D mutation suggest that factors other than the formation of known four-helix bundles can cause the two chromophores to approach. The linker region (L in Fig. 1A) may be this factor. It includes palmitoylated cysteines, a conserved membrane-targeting domain Gln-Pro-Ala-Arg-Val (*21*), and a stretch of basic amino acids alternating with hydrophobic residues (Lys-Leu-Lys-Ser-Ser-Asp-Ala-Tyr-Lys-Lys-Ala-Trp). In other proteins, including Syb and Syx, such stretches often interact with lipid bilayers (*22–24*). Thus much or all of the linker region is probably bilayer associated in vivo

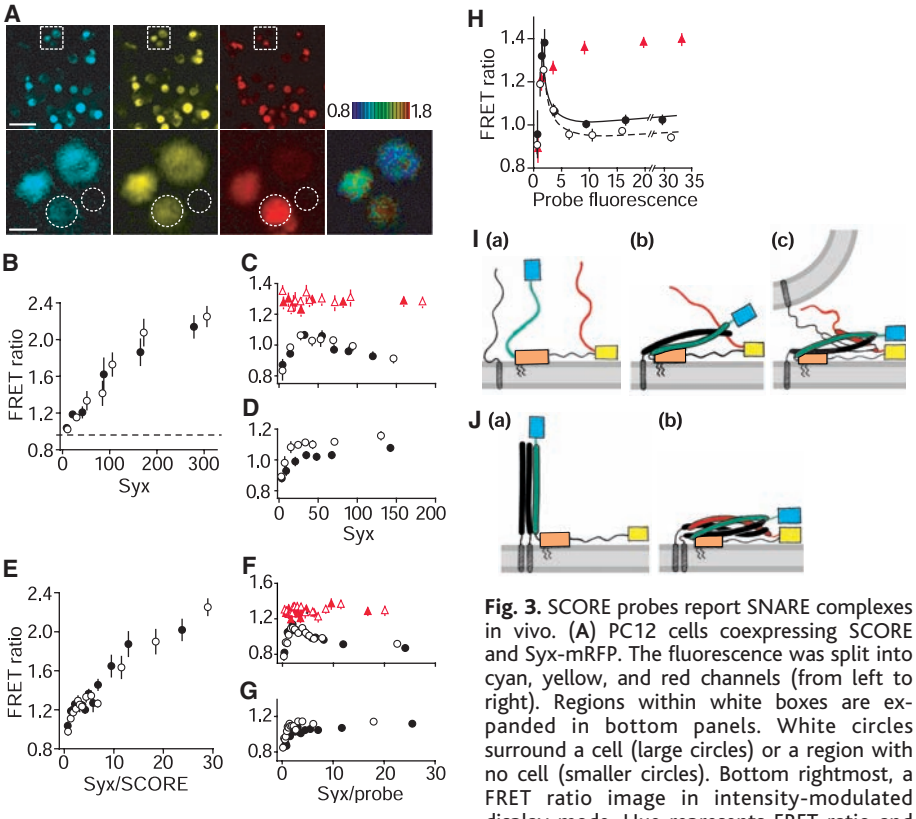


**Fig. 3.** SCORE probes report SNARE complexes in vivo. (**A**) PC12 cells coexpressing SCORE and Syx-mRFP. The fluorescence was split into cyan, yellow, and red channels (from left to right). Regions within white boxes are expanded in bottom panels. White circles surround a cell (large circles) or a region with no cell (smaller circles). Bottom rightmost, a FRET ratio image in intensity-modulated display mode. Hue represents FRET ratio and the brightness is proportional to the average of cyan and yellow fluorescence. Scale bars, 50 μm (top) and 10 μm (bottom). (**B** to **D**) FRET ratios as a function of Syx-mRFP fluorescence. The dashed line in (B) indicates the FRET ratio of uncomplexed SCORE (*29*). Cells coexpressed Syx constructs with SCORE (B), ΔSN1 (red triangles) or ΔSN2 (black circles) (C), or ΔSN2-G43D (D). Cells were selected to have probe fluorescence values of 3 to 20. Each data point is an average of 8 to 20 points with similar abscissa values. Filled symbols show Syx-mRFP and open symbols show Syx-ΔNT-mRFP. (**E** to **G**) Similar to (B) to (D) except that the complete data set was included, and FRET ratios were plotted against the ratio of Syx fluorescence divided by probe fluorescence. Probe fluorescence had values of 3 to 100 for 94% of cells. (**H**) Cells expressed SCORE (filled circles), ΔSN2 (open circles), or ΔSN1 (red triangles), but no exogenous Syx. Location of the cells was determined from brightfield micrographs. Fluorescence of the dimmest cells (values <1.0) was attributed to autofluorescence. (**I**) Syx (black) and SN1 (green) (a) form a precursor lying nearly flat on the membrane (b). SNARE motifs are drawn as a two-helix bundle. (c) Nascent core complex. White, Syb; red, SN2; blue box, CFP; orange box, bilayer-associated portion of the linker domain; yellow box, Venus. (**J**) Complexes at high concentration of Syx. (a) Without SN2, Syx dimers (*30*) bind ΔSN2 in a complex that competes with precursor and is silent because it separates the chromophores. G43D disrupts the silent complex, restoring precursor and partial FRET. (b) Without vesicles, precursor forms the binary $(Syx)_2$-SNAP25 complex, possibly via an intermediate analogous to (c) in (I). It generates full FRET but may be rare in untransfected cells because it requires high Syx concentration. Errors bars in (B) to (H) show mean ± standard error.

(Fig. 3Ia). Such association may give it sufficient structure (orange box) to bind a complex of Syx and SN1 (Fig. 3Ib). Inasmuch as such binding diminishes the average distance between CFP and Venus, the model explains both partial FRET and its absence in solution. This or a related structure (Fig. 3Ib) could well be a precursor for the exocytic core complex. Beneath a docked vesicle, the free SN2 region would be well positioned to capture the N terminus of Syb (Fig. 3Ic), thus initiating formation of the core complex. Where there are no vesicles, the precursor may form four-helix bundles with Syx (Fig. 3Jb). When SN2 is missing, a silent complex (Fig. 3Ja) competes with the precursor.

The amount of any precursor complex is expected to increase, at least transiently, when cytosolic [$Ca^{2+}$] causes the priming of new secretory vesicles for exocytosis. Thus, partial FRET should increase when cells are stimulated. Indeed, the FRET ratio rose and fell while external [$K^+$] was raised and lowered in neurites of differentiated PC12 cells (Fig. 4, A and B). The effect required external $Ca^{2+}$, consistent with a requirement for $Ca^{2+}$ entry through voltage-gated Ca channels. As in Fig. 3, C and D, the FRET change was due neither to the binary complex $(Syx)_2$-SNAP25 (*3*) nor to known Syx-ΔSN2 complexes (*5*, *17*), given that it was observed with both ΔSN2 and ΔSN2 G43D. It required Syx because it was absent in cells coexpressing *Botulinus* neurotoxin C (BoNT/C) light chain, a Syx-selective protease. No FRET change was seen with ΔSN1.

We next assayed exocytosis, another process requiring the entry of $Ca^{2+}$. In cells expressing neuropeptide Y (NPY)–mRFP, external [$K^+$] caused neurites to dim as cells released this granule marker (Fig. 4C) (*25*). Similar to the FRET change, peptide release required external [$Ca^{2+}$] and was diminished when BoNT/C cleaved Syx (Fig. 4D). Apparently, $Ca^{2+}$ influx through voltage-gated Ca channels caused exocytosis as well as FRET, and both effects required Syx. However, the FRET change did not require the formation of exocytic core complex, as it was observed also in cells coexpressing tetanus toxin (TeTx) light chain (Fig. 4E). This Syb-specific protease strongly inhibited exocytosis (*26*) in parallel NPY release assays (Fig. 4F).

Finally, we observed neurites under evanescent field illumination (total internal reflection fluorescence), a method that selectively illuminates the plasma membrane where cells adhere to a glass coverslip (*27*, *28*). As under epifluorescence, raising external [$K^+$] caused a reversible increase in FRET that required external $Ca^{2+}$ (Fig. 4G and fig. S2). The signal was twice as large as under epifluorescence, consistent with a disproportionally large contribution from the plasma membrane.

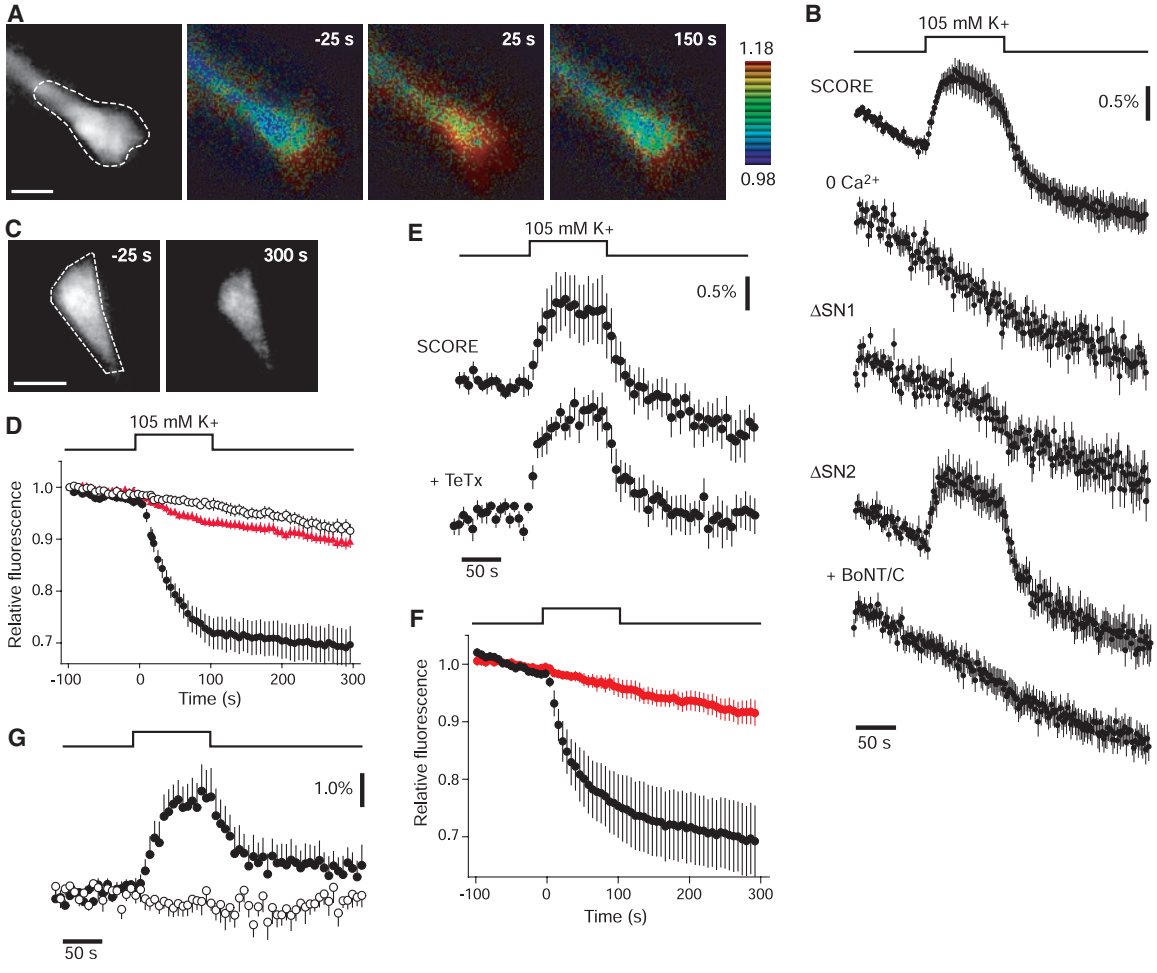


**Fig. 4.** Voltage-gated $Ca^{2+}$ entry promotes the formation of Syx-SN1 complexes. (**A**) Cyan fluorescence (leftmost) and FRET in a neurite from a differentiated PC12 cell expressing SCORE. FRET images were taken at the indicated times relative to a 100-s-long elevation of external [$K^+$]. External [$Ca^{2+}$] = 50 mM throughout for more reliable stimulation (*31*, *32*). Regions (dashed outlines) were analyzed as in Fig. 3A to obtain spatially averaged FRET ratios; background subtraction was based on fluorescence in a nearby circle similar in size to the neurite. Scale bar, 10 μm. (**B**) Percentage of changes in FRET ratio while [$K^+$] (uppermost) was raised and lowered. Traces are averages of 16 to 25 cells each with SCORE, SCORE and no external [$Ca^{2+}$], ΔSN1, ΔSN2, and ΔSN2 coexpressed with BoNT/C light chain. (**C**) NPY-mRFP containing neurite before and after elevated [$K^+$]. Scale bar, 10 μm. (**D**) NPY release. Fluorescence intensity [dashed outline in (C)] corrected for background and plotted against time (filled circles). Data from each neurite were scaled to the values before [$K^+$] was changed; the results were then averaged (9 to 28 cells). The fluorescence decline signals release of NPY-mRFP. Open circles, as above but with no external $Ca^{2+}$. Red triangles, as for filled circles but in cells coexpressing BoNT/C. (**E**) As in (B) but cells contained SCORE, either alone or coexpressed with TeTx light chain. (**F**) As in (D) but cells contained NPY-mRFP, either alone (8 cells, black) or coexpressed with TeTx (11 cells, red). (**G**) Plasma membrane FRET changes recorded with total internal reflection fluorescence. SCORE expressing cells were bathed in a solution containing 50 mM (filled circles) or no external [$Ca^{2+}$] (open circles). Note different ordinate scale. Error bars in (B) and (D) to (F) show mean ± standard error.

In conclusion, a SNARE complex with previously unrecognized properties formed in a $Ca^{2+}$-dependent manner from a saturable pool of Syx. Compared with previous candidates for the core complex precursor, it formed in the absence of SN2 (*5*). It may be the plasma membrane "receptor" for Syb when vesicles dock.

**References and Notes**


1. P. I. Hanson, R. Roth, H. Morisaki, R. Jahn, J. E. Heuser, *Cell* **90**, 523 (1997).
2. R. B. Sutton, D. Fasshauer, R. Jahn, A. T. Brunger, *Nature* **395**, 347 (1998).
3. D. Fasshauer, W. K. Eliason, A. T. Brunger, R. Jahn, *Biochemistry* **37**, 10354 (1998).
4. T. Weber *et al.*, *Cell* **92**, 759 (1998).
5. C. Rickman *et al.*, *J. Biol. Chem.* **279**, 644 (2004).
6. Y. A. Chen, S. J. Scales, R. H. Scheller, *Neuron* **30**, 161 (2001).
7. A. Miyawaki, R. Y. Tsien, *Methods Enzymol.* **327**, 472 (2000).
8. D. Fasshauer, H. Otto, W. K. Eliason, R. Jahn, A. T. Brunger, *J. Biol. Chem.* **272**, 28036 (1997).
9. W. Xiao, M. A. Poirier, M. K. Bennett, Y. K. Shin, *Nature Struct. Biol.* **8**, 308 (2001).
10. K. L. Nicholson *et al.*, *Nature Struct. Biol.* **5**, 793 (1998).
11. T. Nagai *et al.*, *Nature Biotechnol.* **20**, 87 (2002).
12. D. Fasshauer, W. Antonin, V. Subramian, R. Jahn, *Nature Struct. Biol.* **9**, 144 (2002).
13. The ΔSN2 mutant retains the SN1 region, which complexes with Syx and forms four-helix bundles with the stoichiometry $(Syx\text{-}SN1)_2$ (*17*). The parallel orientation of ΔSN2 in such complexes would bring CFP into proximity not with Venus but with another CFP, possibly favoring nonfluorescent energy transfer between two CFPs. The complex would also hinder the approach of CFP and Venus that might occasionally occur by thermal flexing of unstructured SCORE. Both effects would tend to diminish FRET.
14. R. E. Campbell *et al.*, *Proc. Natl. Acad. Sci. U.S.A.* **99**, 7877 (2002).
15. All constructs were found not only in the plasma membrane but also inside the cell, especially when strongly overexpressed. However, the proportion of SCORE inside cells did not vary systematically between different SCORE mutants (fig. S1).
16. D. Fasshauer, D. Bruns, B. Shen, R. Jahn, A. T. Brunger, *J. Biol. Chem.* **272**, 4582 (1997).
17. K. M. Misura, L. C. Gonzalez Jr., A. P. May, R. H. Scheller, W. I. Weis, *J. Biol. Chem.* **276**, 41301 (2001).
18. P. I. Hanson, H. Otto, N. Barton, R. Jahn, *J. Biol. Chem.* **270**, 16955 (1995).
19. T. Lang, M. Margittai, H. Holzler, R. Jahn, *J. Cell Biol.* **158**, 751 (2002).
20. In the very dimmest cells, autofluorescence resulted in an apparent FRET ratio of 1 with all three probes. At higher probe concentrations, the influence of autofluorescence waned, as documented by the Syx-insensitive probe SCORE ΔSN1, whose FRET values approached those seen under other conditions (Fig. 3, C and F).
21. S. Gonzalo, W. K. Greentree, M. E. Linder, *J. Biol. Chem.* **274**, 21313 (1999).
22. J. A. Killian, G. von Heijne, *Trends Biochem. Sci.* **25**, 429 (2000).
23. D. H. Kweon *et al.*, *Biochemistry* **41**, 5449 (2002).
24. K. Hu *et al.*, *Nature* **415**, 646 (2002).
25. X. Lu, G. C. Ellis-Davies, E. S. Levitan, *Cell Calcium* **33**, 267 (2003).
26. X. Huang *et al.*, *Am. J. Physiol. Cell Physiol.* **281**, C740 (2001).
27. D. Axelrod, *J. Biomed. Opt.* **6**, 6 (2001).
28. J. A. Steyer, W. Almers, *Nature Rev. Mol. Cell Biol.* **2**, 268 (2001).
29. Purified SCORE (10 μM) was pulled up into a glass microcuvette (20-μm path length, Vitro Dynamics, New York), whose ends were then sealed with vaseline. The cuvette was placed under a drop of water and imaged as if it were a cell.
30. J. C. Lerman, J. Robblee, R. Fairman, F. M. Hughson, *Biochemistry* **39**, 8470 (2000).
31. The FRET with SCORE was also observed in 2 mM external $[Ca^{2+}]$.
32. Materials and methods are available as supporting material on *Science* Online.


33. We thank J. Adelman, C. Bond, and S. Bae for help. Supported by NIH MH60600. Molecular interaction data have been deposited in the Biomolecular Interaction Network Database with accession codes 180392 and 180393.


**Supporting Online Material**

www.sciencemag.org/cgi/content/full/306/5698/1042/DC1
Materials and Methods
Figs. S1 and S2
References

9 July 2004; accepted 8 September 2004

# A Link Between mRNA Turnover and RNA Interference in *Arabidopsis*

**S. Gazzani,[1]* T. Lawrenson,[1]* C. Woodward,[2] D. Headon,[3] R. Sablowski[1]†**

**In RNA interference (RNAi), double-stranded RNA (dsRNA) triggers degradation of homologous messenger RNA. In many organisms, RNA-dependent RNA polymerase (RdRp) is required to initiate or amplify RNAi, but the substrate for dsRNA synthesis in vivo is not known. Here, we show that RdRp-dependent transgene silencing in *Arabidopsis* was caused by mutation of XRN4, which is a ribonuclease (RNase) implicated in mRNA turnover by means of decapping and 5′-3′ exonucleolysis. When both XRN4 and the RdRp were mutated, the plants accumulated decapped transgene mRNA. We propose that mRNAs lacking a cap structure become exposed to RdRp to initiate or maintain RNAi.**

RNA interference is a conserved posttranscriptional control mechanism that is initiated by dsRNA and causes degradation of mRNAs with homology to the dsRNA trigger. The dsRNA is cut by the Dicer RNase into 21- to 25-nucleotide (nt) fragments, called small interfering RNAs (siRNAs). The siRNAs are incorporated into the RNA-induced silencing complex (RISC), which uses them as a guide to identify and to degrade matching mRNAs (*1*).

RNA interference can be triggered by viral dsRNA, by self-complementary transcripts, or by sense transgenes, a phenomenon also called cosuppression (*2*, *3*). Cosuppression can be triggered by complex transgene insertions, which may produce antisense or self-complementary transcripts, or by single transgenes with high expression levels (*4*). In the case of single, sense transgenes, it has been proposed that aberrant transcripts (e.g., caused by premature transcriptional termination) could be converted to dsRNA by RNA-dependent RNA-polymerases (RdRps), which are required for RNAi in plants, fungi, and *Caenorhabditis elegans* (*5*–*9*). The RdRps are also believed to amplify and to maintain RNAi, by using siRNAs as primers to synthesize new dsRNA (*10*). In both the initiation and amplification of RNAi, however, the template used by RdRp in vivo is unknown.

Here, we have isolated an *Arabidopsis* mutant that promotes RdRp-dependent cosuppression and show that the corresponding wild-type gene encodes an RNA exonuclease that likely degrades the template for RdRp. The mutant was isolated (*11*) in a screen for suppressors of a single-copy transgene expressing a fusion between SHOOT MERISTEMLESS (STM, a regulator of meristem development) (*12*), and the rat glucocorticoid receptor (GR), under the widely expressed 35*S* promoter. Activation of STM-GR with dexamethasone (DEX) activates meristem genes and inhibits cotyledon and leaf development (Fig. 1, A and B) (*13*). The recessive *xrn4-1* mutation suppressed this phenotype (Fig. 1, C and D). When *xrn4-1, STM-GR* was crossed with the wild type lacking *STM-GR*, all progeny showed the DEX-induced *STM-GR* phenotype, so the transgene was intact. Suppression in trans was also confirmed by segregating *xrn4-1* from the transgene and, after three backcrosses with the wild type, crossing again with *STM-GR*.

In a homozygous *STM-GR* background, *xrn4-1* segregated as a single locus. In *xrn4-1* plants that were hemizygous for *STM-GR*,

[1]Cell and Developmental Biology, John Innes Centre, Norwich NR4 7UH, UK. [2]Department of Biology, University of Washington, Seattle, WA 98195–5325, USA. [3]School of Biological Sciences, University of Manchester, Manchester M13 9PT, UK.

*These authors contributed equally to this work.
†To whom correspondence should be addressed. E-mail: robert.sablowski@bbsrc.ac.uk